**Biopolymers:
Peptide Science**
WILEY

Conformation, Self-aggregation, and Membrane Interaction of Peptaibols as Studied by Pulsed Electron Double Resonance (PELDOR) Spectroscopy

SCHOLARONE™
Manuscripts

Review

Conformation, Self-aggregation, and Membrane Interaction of Peptaibols as Studied by Pulsed Electron Double Resonance (PELDOR) Spectroscopy

Alexander D. Milov,[1] Yuri D. Tsvetkov,[1] Jan Raap,[2] Marta De Zotti,[3] Fernando Formaggio,[3] Claudio Toniolo[3]

[1] *V.V. Voevodsky Institute of Chemical Kinetics and Combustion, 630090 Novosibirsk, Russian Federation*

[2] *Leiden Institute of Chemistry, Gorlaeus Laboratories, Leiden University, 2300 RA Leiden, The Netherlands*

[3] *Department of Chemistry, University of Padova, 35131 Padova, Italy*

Correspondence to: Prof. Claudio Toniolo, Department of Chemistry, University of Padova, via Marzolo 1, 35131 Padova, Italy; e-mail: claudio.toniolo@unipd.it or to
Prof. Yuri D. Tsvetkov, V.V. Voevodsky Institute of Chemical Kinetics and Combustion, Russian Academy of Sciences (Siberian Branch), Institutskaya 3, 630090 Novosibirsk, Russian Federation; e-mail: tsvetkov@kinetics.nsc.ru

ABSTRACT

Pulsed EPR methods, in particular PELDOR (or DEER), are very sensitive to the dipole⋯dipole interaction between electron spins in a pair of free radicals. Using PELDOR, the conformations of a number of double radical-containing biomolecules have been determined. In this review article we focused our attention on the application of this spectroscopy to nitroxide-labeled peptaibols. This is an emerging class of naturally-occurring, relatively short, linear, helical peptide molecules endowed with hydrophobic character, capability to interact with and to alter the structure of membranes, and antibiotic activity. We extracted detailed information on the secondary structures of specifically site-directed, double nitroxide-labeled peptaibols under a variety of experimental conditions, including biologically relevant environments. Moreover, we examined in depth peptaibol clustering, related to the marked propensity of these molecules to undergo self-association in model and whole-cell membrane systems, using mainly mono nitroxide-containing synthetic analogs. Finally, based on the PELDOR data accumulated, we proposed models of supramolecular (quaternary) structures of peptaibols and their binding modes to membranes.

Keywords: membranes; PELDOR spectroscopy; peptaibol; peptide conformation; peptide self-association

INTRODUCTION

Pulsed electron double resonance (PELDOR), also termed double electron-electron resonance (DEER) (the former abbreviation is used hereinafter), which was developed in 1981[1] and modified in 2000,[2] is currently considered the most popular pulsed EPR method. It is widely used in 3D-structural studies of systems containing paramagnetic centers.

Reviews that cover the PELDOR theory and provide examples of its application to 3D-structural investigations are published very frequently.[3-8] The most significant success in the research into biomolecules using PELDOR was undoubtedly achieved thanks to the development of effective experimental methods for site-directed spin labeling. This review aims at presenting the results of PELDOR applications in 3D-structural studies of the naturally-occurring class of peptaibols.

Using the PELDOR method, the function of distance distribution between spin labels, $F(r)$, or distance spectrum, can be extracted. In the latter case, the shape of this function can be employed to describe the dispersion in distances due to, for example, a conformational distribution of spin labels.[9,10] As PELDOR experiments are carried out at low (cryogenic) temperatures, it is assumed that the same conformational equilibrium does exist at higher (room) temperature and it is instantaneously fixed as the molecules freeze. This assumption is authenticated by the numerous strict correlations between PELDOR data and molecular dynamics (MD) simulation results obtained, for example, for spin-labeled nitroxides and DNA.[4,11] The distance distribution pattern is characterized by the Δ-value, the width of the $F(r)$ function at the half of its maximum intensity.

Peptaibols are members of a class of largely hydrophobic, membrane-active, linear peptides characterized by a main-chain of up to 21 α-amino acids and endowed of antibiotic activity.[12-22] As their biosynthesis is not a ribosomal process, even nonprotein residues, *e.g.* the C^α-tetrasubstituted α-aminoisobutyric acid (Aib) (Figure 1), may be very frequently found in their primary structure. In turn, Aib is a strongly foldameric residue,[23,24] so it is quite reasonable that peptaibols would adopt helix structures in artificial bilayers and natural membranes where they exert their bioactivities. Peptaibols typically contain an N-terminal acyl (either an acetyl or a long fatty acyl) group and a C-terminal 1,2-amino alcohol which remove positive and negative charges, respectively, from their backbone ends. In Nature, most of them show microheterogeneity, *i.e.* a mixture of closely similar peptides with numerous conservative changes in the sequence.

Information on the 3D-structure and properties of peptaibols and their aggregates is necessary for the design of efficient antibiotics. The PELDOR technique enables revealing 3D-structural peculiarities, including self-assembly, of peptaibols in different membrane-mimicking solvents, in

lipid model systems, and in bacterial whole cells as well. Details could be obtained by measurement of the dipole···dipole interactions between site-directionally introduced spin labels. Due to the fact that our typical nitroxide spin label 4-amino-1-oxyl-2,2,6,6-tetramethylpiperidine-4-carboxylic acid (TOAC, Figure 1)[25] is covalently and rigidly embedded (in the absence of any flexible side-chain linker) in the peptide sequence, the distance between spin labels can be measured accurately. However, its six-membered cyclic system may exist at least in two conformations.[26-28]

Pore formation in biological membranes, which eventually generates cell leakage, is generally believed to be a fundamental principle of antibiotic activity for membrane-active peptides. In this connection, peptaibols are particularly intriguing because many of them show membrane voltage activation.[12,13,15,20-22,29,30] It would be of interest to ascertain why these almost electrically neutral molecules exhibit such a property. Even more challenging is the known observation that they are able to induce membrane leakage even in the absence of voltage activation.
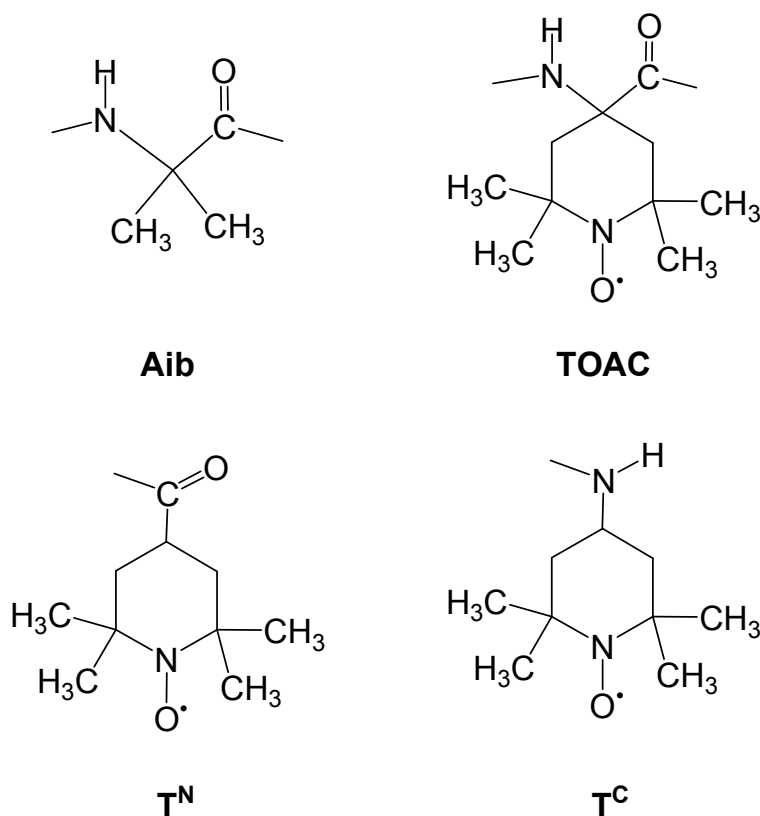

FIGURE 1 Chemical structures of Aib, TOAC, **T^N**, and **T^C**.

In summary, PELDOR, one of the spectroscopies more widely employed to investigate pore formation, is extremely useful to afford information on the overall 3D-structure and self-

association modes of biomolecules in membranes. The application of other spectroscopic techniques, such as fluorescence (in particular, the fluorescence resonance energy transfer, FRET, method) is nonetheless highly desirable, to confirm and further refine the final picture provided by PELDOR data.

PELDOR SPECTROSCOPY

For PELDOR investigations, two spin labels are typically introduced into molecules. Stable nitroxide radicals are commonly used as labels. The dipole and exchange magnetic interactions between the labels contain information regarding distances between the labels, aggregation and complexation of labeled molecules, and spatial distribution of the spin labels in the compound under scrutiny.

Let us first provide the most important information on the PELDOR theory required for the analysis of the results discussed in this review article. The magnetic dipole···dipole and exchange interactions between the A and B spin labels are determined by the PELDOR modulation frequency, ω_m[3,31,32]:

$$\omega_m = \omega_{dd} + J = \frac{D}{r^3}(1 - 3\cos^2\theta) + J \tag{1}$$

Here, ω_{dd} is the dipole···dipole frequency, J is the exchange interaction frequency, D is the dipole···dipole interaction constant, r is the interspin distance (nm), and θ is the angle between the direction of the external magnetic field and the vector connecting the spins. The dipole···dipole constant, D, in convenient units is equal to $2\pi(52.04$ MHz nm$^3)=327$ rad nm^3/μs. In case of neglecting the exchange interaction ($J << D/r^3$), the PELDOR technique is used to determine the dipole frequency ω_{dd} directly and, hence, the distance between the spins.

A three-pulse PELDOR (3p PELDOR) sequence, shown in Figure 2a, consists of two types of pulses at the frequencies ν_A and ν_B. Pulses 1 and 2 ($\pi/2$ and π pulses in the classical spin echo Hahn sequence) at the frequency ν_A acting upon the spins A in the EPR spectrum (Figure 2b) are used to form the spin echo signal, which is then employed to detect the PELDOR effect. The interval τ between the pulses at the frequency ν_A is typically fixed. The pumping pulse π at the frequency ν_B, which acts on the spins B with a delay T, counted from the first $\pi/2$ pulse, lies in this interval. Note that it is assumed that the frequencies of ν_A and ν_B are considerable different to avoid the direct action of the pumping pulse on spins A. The pumping pulse changes the orientation of spins B, resulting in a variation in the dipole interaction between spins A and B. This change is recorded as

the decay of the spin echo signal, $V(T)$, when the delay T varies in the interval $0 - \tau$. The PELDOR time trace $V(T)$ is modulated at the frequency ω_m [relation(1)], which allows one to analyze the interspin distance r. Modulation in the time trace was first observed and investigated in 1984.[33,34] A four-pulse sequence (4p PELDOR) is also used. In this case, a refocused echo signal is formed under the influence of three pulses ($\pi/2$, π, π) at frequency ν_A and a change in it occurs due to the π pumping pulse, which is applied in the interval between the second and third pulses at ν_B.
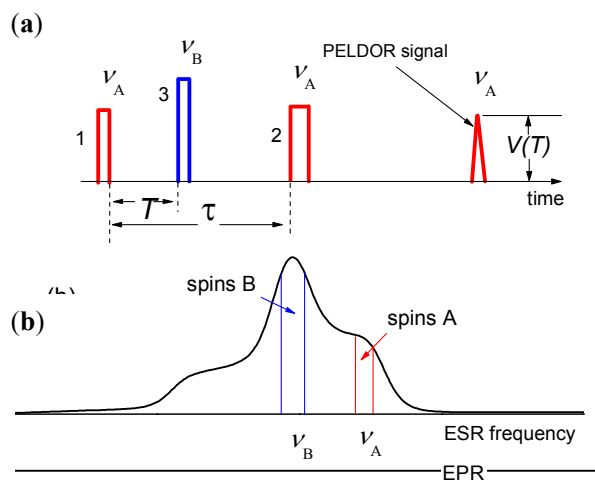

FIGURE 2 (a) 3p PELDOR pulse sequence. The spin echo signal is the result of a two-pulse action at frequency ν_A. When the third pumping pulse at ν_B acts on the spin system, the PELDOR effect which arises can be registered as a T time scale function, $V(T)$. **(b)** Positions of pumping (B) and detection (A) pulses in the EPR frequency spectrum.

The PELDOR time trace for a randomly oriented pair of spin labels with a fixed r under the approximation of short microwave pulses is described by the following relationship[3,31,32]:

$$V(r,T)=V_0(1-p_b\{1-f(r,T)\}) \tag{2}$$

where

$$f(r,T) =< \cos[\ ((\frac{D}{r^3}(1-3\cos^2\theta)+J)\ )T\ ]>_\theta \tag{3}$$

Here, V_0 is the signal value at $T=0$, p_b is the probability of rotation of one of the spins in a pair when the pumping pulse is applied, $<...>_\theta$ denotes the averaging of spin pairs on orientations. The averaging of relationships (2) and (3) over θ yields a decreasing function modulated by attenuating oscillations at frequency ω_{dd} (Figure 3). At $T\rightarrow\infty$, the function $V(T)$ approaches its limiting value

$V_{p.}=V_0(1-p_b)$. A Fourier analysis of this PELDOR time trace yields a so-called Pake pattern, which allows one to obtain data on the distance r and the exchange integral J.[3,31] It is worthwhile to mention that, at distances longer than about 1.2 nm, the J integral is usually negligibly small.[35]
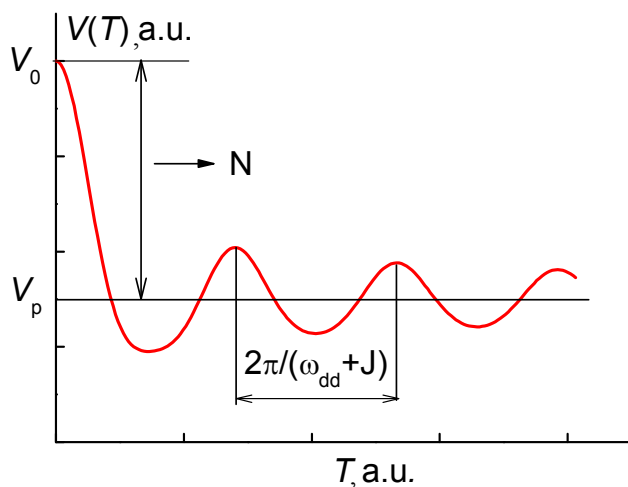

FIGURE 3 Modulated at $(\omega_{dd}+J)$ frequency PELDOR time trace $V(T)$ and its limiting value, V_p, at $T\rightarrow\infty$.

The distance between spin labels in a pair can remain unfixed for different reasons. This phenomenon produces changes in the $V(T)$ function, for example as it is shown in Figure 4.
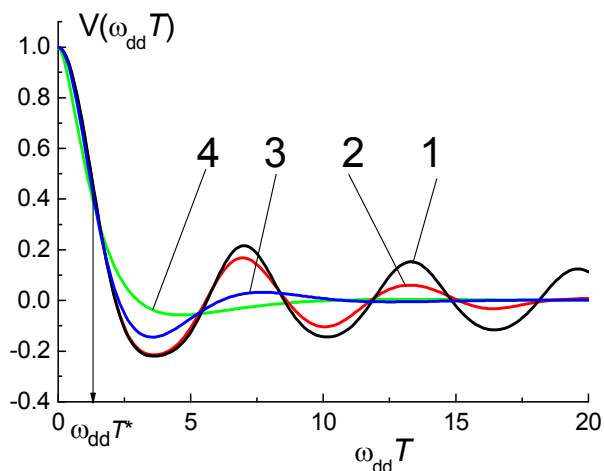

FIGURE 4 Effect of the spread of the spin···spin distance $\Delta r_{AB}/ r_{AB}$ on the PELDOR time trace, $V(T)$.

$\Delta r_{AB}/ r_{AB} = 0$ (1), 0.10 (2), 0.15 (3), 0.25 (4).

In the general case, a distance distribution $F(r)$ between the labels (distance spectrum) $F(r)dr = dn(r)/n$ is introduced, which represents the fraction of spin-label pairs with the distance between the labels in a pair in the range between r and $r+dr$. In the case of a continuous distance distribution, the function describing the PELDOR time trace can assume the following form[3,31,32]:

$$V(T) = V_p + (V_0 - V_p)\int_{r_1}^{r_2} F(r)f(r,T)dr \qquad (4)$$

Experimental PELDOR time traces are conveniently analyzed using the normalized PELDOR signal time trace, $V_n(T)$:

$$V_n(T) = \frac{V(T) - V_p}{V_0 - V_p} = \int_{r_1}^{r_2} F(r)f(r,T)dr \qquad (5)$$

Here, $V(T)$ is the experimental PELDOR trace, V_0 is the same trace at $T=0$. The limits of integration r_1 and r_2 in (4) restrict the physically reasonable range of distances between spin labels. Expression (5) is a first-kind Fredholm equation, the solution of which is unstable due to the inaccuracies in the experimental value $V(T)$. The calculation of $F(r)$ basically reduces to a solution of the inverse problem using the Tikhonov regularization techniques.[36]

The distance distribution function definition in radical pairs from the experimental PELDOR data was developed[37-40] and the method for three spin labels was reported.[41] The program for calculation of $F(r)$ using the PELDOR time traces was provided.[42] The maximum of the function $F(r)$ corresponds to the distance between the spin labels, r, and its width, Δ, specifies the distance distribution of the labels.

Two types of dipole interactions exist in real systems containing spin groups: (i) those between the paramagnetic centers within a group, $V(T)_{INTRA}$, and (ii) those between the paramagnetic centers of different groups, $V(T)_{INTER}$. The dipole interaction within pairs of spin labels was discussed above. If these interactions are considered independent, then the entire function describing the time trace $V(T)$ can be written[31]:

$$V(T) = V(T)_{INTRA} V(T)_{INTER} \qquad (6)$$

In most cases, PELDOR is used to investigate systems of spin labels or groups of labels which are uniformly distributed over a volume. The PELDOR time trace for paramagnetic centers randomly distributed over a 3D-space can be described using the exponential function:[3]

$$V_{INTER}(T) = V(0)exp[-2p_b\Delta\omega_{1/2}T] = V(0)exp[-\alpha T^{4/3}] \qquad (7)$$

8

where $\Delta\omega_{1/2}$= $8.2 \times 10^{-13} \cdot C \cdot cm^3 \cdot s^{-1}$ is the dipole width, and C is the concentration of the paramagnetic centers (in cm^{-3}). In general, the α and A values depend on the spatial dimensions. For instance, $A = 3$ for a 3D-space, $A = 2$ for a plane, and $A = 1$ for a line.[3,31] The α and A values can be calculated also for more complex situations of spatial distribution of paramagnetic centers.[43] A comparison of the experimentally determined and the estimated α and A values opens the doors to investigating the features of the spatial distribution using PELDOR.

In many cases, spatial clusters or aggregates of spin labels may be formed. If it is assumed that all aggregates under investigation are identical and that each of them contains N paramagnetic molecules, the PELDOR time trace due to dipole$\cdots$dipole coupling of spins within (intra) the aggregates will have the form[3,31,44]:

$$V(T)_{INTRA}=V(0)[1-p_b<1-\cos(DT)>_{\vartheta,r}]^{N-1} \tag{8}$$

where $V(T)_{INTRA}$ is the PELDOR signal decay function, and $<...>_{\vartheta,r}$ indicates averaging over all possible values of angles and distances between labels within the aggregate.

Averaging in (8) due to a random orientation of aggregated molecules provides a fast decay of the echo signal at time $T \leq T^*$, corresponding to the value of the mean dipolar coupling of spins and effective distance $R_{eff}=(DT^*)^{1/3}$. Function (8) tends to its limit V_p at $T \geq T^*$. The V_p value can be obtained from eq. (8) at $<\cos(DT)>=0$. At small p_b values:

$$V_p=V(0)(1-p_b)^{N-1}\cong 1-(N-1)p_b \tag{9}$$

Equation (9) makes it possible to estimate the number of spin labels in the aggregate, N. To this end, it is necessary to know either the V_p or p_b values.

Recent developments of the theory of the PELDOR method include the use of more accurate theoretical formulas[32,45] for the analysis of the experimental results. Newly proposed aspects of a sophisticated PELDOR theory[46,47] take into account the interaction between spin labels in pairs or aggregates when the EPR spectra of spins A and B overlap or coincide. In this case, corrections for theoretically calculated p_b values are needed. If these corrections are disregarded, a systematic error will be introduced, but it will not be higher than 5-10%[46] in the calculated number of spins (N) in aggregates. If the parameter p_b is determined from experiment (see below), N is free from this error.

Modern PELDOR theory and experimental techniques allow one to obtain 3D-structures and self-aggregation properties of biologically important molecules. The results of our investigation using this method on peptaibols are summarized and discussed later in the text.

Based on the theoretical relationships presented above, we followed this order of analysis of our PELDOR experimental data:

1. Separation of the contributions $V(T)_{inter}$ and $V(T)_{intra}$ from the initial PELDOR time trace $V(T)$.

2. Conclusions on specific features of the spatial distribution of the paramagnetic molecules based on the $V(T)_{inter}$ time trace.

3. Identification of aggregates *via* $V_n(T)_{intra}$, determination of the number of molecules in the aggregates, and evaluation of distances from the Fourier analysis.

4. Calculations of the normalized time trace $V_n(T)$ using the experimental V_p.

5. Calculations of the distance spectra $F(r)$.

SPIN-LABELED PEPTAIBOLS: SECONDARY STRUCTURES

STUDIES IN FROZEN GLASSY SOLUTIONS

Using PELDOR spectroscopy, a variety of site-directed (both mono- and double-) labeled peptaibols of largely divergent main-chain length (Figure 5), prepared by chemical synthesis, were studied by our groups in frozen glassy solutions. For spin labeling, in almost all cases one or two Aib residues[23,24] were replaced by the equally efficient helicogenic TOAC residues[25] (Figure 1) characterized by a stable nitroxide (free radical) in its side chain. Exceptions are the two zervamicin analogs that were labeled with the TEMPO derivatives **T**$^{\mathbf{N}}$ and **T**$^{\mathbf{C}}$,[48,49] shown in Figure 1 at their N- or C-terminus, respectively. Millhauser and Toniolo[26-28] were the first to introduce an approach which correlates peptide conformation and experimental distance between two TOAC labels. They used cw ESR, that is valuable for short distances (less than 15 Å) only.

1
2
3
4
5
6
7
8
9
10
11
12
13
14
15
16
17
18
19
20
21
22
23
24
25
26
27
28
29
30
31
32
33
34
35
36
37
38
39
40
41
42
43
44
45
46
47
48
49
50
51
52
53
54
55
56
57
58
59
60

1. Oct[a]-**Aib**[1b]-Gly-Leu-**Aib**[4]-Gly-Gly-Leu-**Aib**[8]-Gly-Ile-Leu-OMe	trichogin GA IV[c] (**O-Tri**)
2. Fmoc-**Aib**[1]-Gly-Leu-**Aib**[4]-Gly-Gly-Leu-**Aib**[8]-Gly-Ile-Leu-OMe	trichogin GA IV[c] (**F-Tri**)
3. Ac-Trp-Ala-**Aib**[3]-Aib-Ala-Gln-Ala-**Aib**[8]-Ser-Aib-Ala-Leu-**Aib**[13]-Gln-Lol	tylopeptin B[c] (**Tyl**)
4. Ac-Phe-**Aib**[2]-Aib-Aib-Val-Gly-Leu-Aib-Aib-Hyp-Gln-Aib-Hyp-**Aib**[14]-Phol	heptaibin (**Hep**)
5. Ac-Trp-Ala-**Aib**[3]-Aib-Leu-Aib-Gln-Aib-Aib-Aib-Gln-Leu-**Aib**[13]-Gln-Leu-OMe	ampullosporin A[c] (**Amp**)
6. Ac-Trp-Ile-Gln-Aib-Ile-Thr-Aib-Leu-Aib-Hyp-Gln-Aib-Hyp-Aib-Pro-**T**[C]	zervamicin IIa[c] (**Zrv-T**[C])
7. **T**[N]-Trp-Ile-Gln-Aib-Ile-Thr-Aib-Leu-Aib-Hyp-Gln-Aib-Hyp-Aib-Pro-**T**[C]	zervamicin IIa[c] (**T**[N]-**Zrv-T**[C])
8. Ac-**Aib**[1]-Pro-Aib-Ala-Aib-Ala-Glu(OMe)-**Aib**[8]-Val-Aib-Gly-Leu-Aib-Pro-Val-**Aib**[16]-Aib-Glu(OMe)-Glu(OMe)-Phol	alamethicin F50/5[c] (**Alm**)
9. Ac-**Aib**[1]-Gly-Leu-Aib-Gly-Gly-Leu-Aib-Gly-Ile-Leu-Aib-Gly-Leu-Aib-Gly-Gly-Leu-**Aib**[19]-Gly-Ile-Leu-OMe	trichogin GA dimer[c] (**D-Tri**)

[a] Other abbreviations used: Oct, 1-octanoyl; OMe, methoxy; Fmoc, 9-fluorenylmethoxycarbonyl; Ac, acetyl; Lol, leucinol; Hyp, (4R)-hydroxy Pro; Phol, phenylalaninol; **T**[c], 4-amino-TEMPO; **T**[N], 4-carboxy-TEMPO; Glu(OMe), γ-methyl Glu.

[b] The Aib residues replaced by TOAC in the labeled analogs studied are given in bold characters.

[c] Analog.

FIGURE 5 Amino acid sequences of the peptaibols investigated by PELDOR spectroscopy.

In polar solvents, such as alcohols, peptaibols are in the monomeric state, while in nonpolar solvents these amphipathic peptides usually self-aggregate. This property offers interesting prospects for their 3D-structural investigation and the study of their supramolecular aggregates in different environments. Information about the secondary structure of peptaibols in the monomeric state as well as in the aggregated state can be obtained from PELDOR spectroscopy by using samples of double spin-labeled peptides. Moreover, we used mono spin-labeled peptides for resolving the global quaternary structure of their aggregates. In all of these experiments, one should first ascertain that the $V(T)_{intra}$ part of the PELDOR time trace for labels within the molecule is separated from the $V(T)_{inter}$ part.

The procedure to determine peptide conformation from PELDOR data is as follows. Assuming that the double labeled peptide is monomerically dissolved in a glassy polar solution, modulation of the PELDOR signal will provide a distance distribution spectrum $F(r)$ between the two labels. Details of the procedure have been described earlier in the theoretical section. After that analysis, it is possible to compare the experimental distance with the calculated distances between label sites for different peptide conformations. The conformational space of peptides is restricted to a set of ϕ and ψ backbone torsion angles defining the α-, 3_{10}-, 2.2_7- (multiple γ-turns) helices and β-sheet conformations.[23,24,50-54] These helices are characterized by different H-bonding patterns related to the relative positions of the C=O and N-H groups, i.e. 2.2_7-helix: $i+2 \rightarrow i$; 3_{10}-helix: $i+3 \rightarrow i$; and α-helix: $i+4 \rightarrow i$. In proteins, 3_{10}-helices have been proposed to be kinetic intermediates in the folding and unfolding processes of long α-helices.[55,56] At the approximate level of heptamers, these two helix conformations appear equally probable.[23,24,50,57] Many, very short, Aib-rich peptides are even known to prefer the 3_{10}-helix. In parallel with these H-bonding

patterns, the length of the different conformations for a given peptide increases in the order α- < 3_{10}- < 2.2_7- < β-sheet. We used this property for the conformational analyses described later in the text by measurement of the distances between amino acids. Calculated distances for different conformations are shown in Figure 6.[49] It is worth mentioning here that the distance between two label sites in a globally unordered conformation might be shorter than in well-defined helices, but only if the intervening peptide linker includes a turn, a loop, or an hairpin local structure.
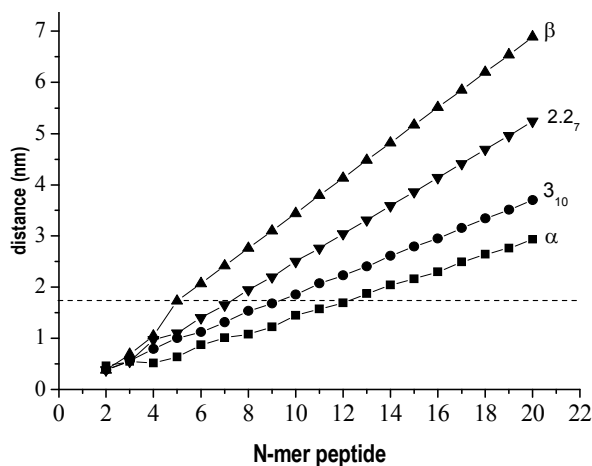

FIGURE 6 Distances between the C^α atoms of the terminal residues of an N-mer peptide calculated for standard α-, 3_{10}-, and 2.2_7-helix and β-sheet conformations. PELDOR measurements of distances are reliable (with an accuracy of ± 0.03 nm) within the range of 1.7 (dashed line) - 8 nm. Qualitative information about shorter distances can be obtained by cw ESR spectroscopy. The latter technique, however, is not suitable to measure longer distances due to a strong inhomogeneous broadening of the spectra.

Trichogin GA IV

In a previous paper,[28] cw ESR spectra of trichogin GA IV were recorded at $g = 4.0$, at half-field in frozen glassy solutions. It was reported that this short 11-amino acid residue lipopeptide can overwhelmingly exist in a mixed α/3_{10}-helical conformation. The same type of mixed helical conformation was found in the crystal state by X-ray diffraction analysis for both trichogin GA IV and **O-Tri[4,8]**.[18,19] From PELDOR data,[58-60] however, it was shown that **O-Tri[1,8]** adopts a conformation dependent upon the nature of solvent (Table I). For instance, in frozen methanol (MeOH) as well as in $CHCl_3$/dimethylsulfoxide (DMSO) (7:3) the experimental distance r=1.97 nm was correlated with the 2.2_7/3_{10}-helices, while in 2,2,2-trifluoroethanol (TFE) a shorter distance (r=1.53 nm) is appropriate for a 3_{10}-helix.[59] Similar results were authenticated by use of cw ESR.[26] In this connection, it is worth noting that the ribbon-like conformation (2.2_7-helix) is rather unusual.[54]

Table I Conformation[a] and Its Dependence on Solvent Polarity, and the Oligomeric Number for Double Spin-Labeled Peptaibol Analogs of Different Length

Peptaibol Analog	Solvent	Oligomeric Number, N	Distance, r (nm)	Δ (nm)	Helix Conformation	Ref.
O-Tri[1,8]	CHCl$_3$/toluene 7:3	4	1.57		3_{10}	60
O-Tri[1,8]	CHCl$_3$/DMSO, MeOH	1	1.97		$2.2_7/3_{10}$[b]	58,59
O-Tri[1,8]	TFE	1	1.53		3_{10}	59
Tyl[3,13]	MeOH/ethanol 95:5	2	1.76	0.07	α	61,62
Hep[2,14]	MeOH/ethanol 95:5	2	2.30	0.07	3_{10}	61,62
Amp[3,13]	MeOH	1	1.73	0.05	α	63
T[N]-Zrv-T[C]	MeOH	2	3.20	0.3[c]	$\alpha/3_{10}$[b]	48,49
Alm[1,16]	MeOH/toluene 1:4	8	2.1	0.3[c]	α	64,65
D-Tri[1,19]	MeOH	1	2.8/3.2	2	$\alpha, 3_{10}$[b]	66,67
D-Tri[1,19]	MeOH/toluene, CHCl$_3$/toluene	2	2.8	0.3	α	66,67

[a] Determined for the segment Aib[i] - Aib[j] from TOAC[i] to TOAC[j] (at 77K). [b] The notations $2.2_7/3_{10}$ and "α / 3_{10}" stand for mixed conformations within *each* molecule, while "$\alpha, 3_{10}$" is used for a mixture of conformations from *different* molecules. [c] Asymmetric distance distributions due to the slightly increased flexibility of the **T[C]** and **T[N]** labels.

Using PELDOR, the conformation can be also determined for peptides in the aggregated state. To avoid intermolecular dipole$\cdots$dipole interactions, the double spin-labeled peptide must be diluted with its unlabeled counterpart. For instance, **O-Tri[1,8]** was found to be 3_{10}-helical in the aggregated state.[60] It may be concluded that short peptaibols such as trichogin exhibit

conformational flexibility, depending upon temperature and nature / organization of the surrounding molecules within the matrix (glass state, crystalline state, etc.). In any case, it is fair to mention that: (i) below $r = 1.70$ nm (Figure 6) a discrimination between the 2.2_7- and 3_{10}-helices is not clear cut and (ii) in our early trichogin investigations we did not employ the improved method of calculation of the distance distribution spectra $F(r)$ that will be discussed later in the text for the other peptaibols.

Tylopeptin B, Heptaibin, and Ampullosporin A

The distance distribution spectrum $F(r)$ for the tylopeptin B (a 14-amino acid residue peptide) analog **Tyl**[3,13] shows a single Gaussian line form[61,62] ($r_{max} = 1.76$ nm, Figure 7A and Table I). The main part of the spectrum for the heptaibin (also a 14-amino acid residue peptide) analog **Hep**[2,14] has also a Gaussian shape, but the less-intense broad line is shifted to longer intramolecular distances ($r_{max} = 2.3$ nm, Figure 7A and Table I).[61,62] Within a reasonable accuracy, **Hep**[2,14] is folded essentially in a 3_{10}-helix conformation. **Tyl**[3,13], on the other hand, seems to adopt a largely prevailing α-helix conformation. The different helices formed by these two peptaibols, despite being characterized by the same number of amino acids, might be ascribed to the two dipeptide sequence Aib-Hyp occurring only in the heptaibin analog that are particularly favorable for the more elongated 3_{10}-helix.
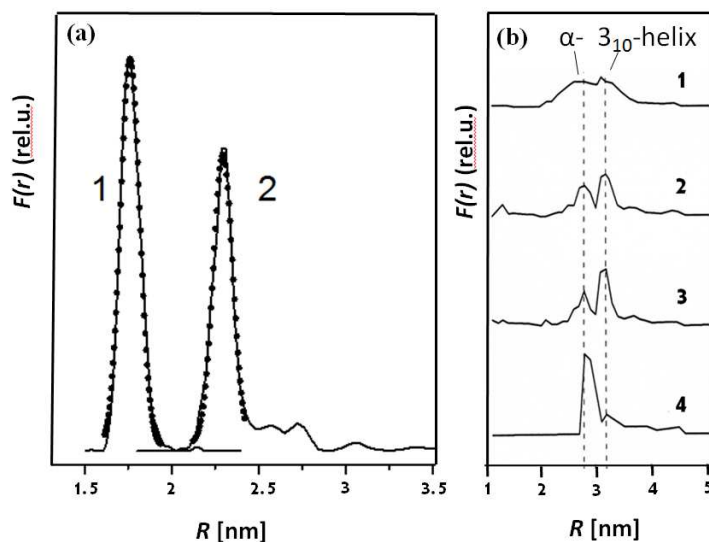

FIGURE 7 Conformation and environment dependencies. (**a**) Intramolecular distance distributions between spin labels for the double spin-labeled peptaibol analogs **Tyl**[3,13] (**1**) and **Hep**[2,14] (**2**) agree with a 3_{10}- and an α-helix conformation, respectively (Table I). (**b**) Changes in the distance distribution function $F(r)$ of **D-Tri**[1,19] upon a change in solvent polarity: MeOH (**1**); toluene-MeOH mixtures containing 10% (**2**) and 20% (**3**) MeOH, and 100% toluene (**4**).

The spin-labeled analog **Amp^{3,13}** of ampullosporin A, an additional medium-length (14-amino acid residue) peptaibol, was studied both by cw ESR and PELDOR.[63] The measurements were achieved in glassy MeOH at 77K. From PELDOR experiments, the distance spectrum exhibits a Gaussian line of the main peak with r_{max} = 1.73 nm (Table I). Similar results were found from cw ESR analysis and by using convolution/deconvolution methods.[68,69] The interspin distance obtained, 1.73 nm, suggests that **Amp^{3,13}** extensively adopts an α-helical structure under these experimental conditions. This conclusion is in very good agreement with that obtained from CD and fluorescence data described in the same paper.[63]

Zervamicin II A

X-Ray diffraction and NMR analysis indicated that zervamicin II A, a slightly longer (15-amino acid residue) peptaibol, is folded in a mixed conformation with an α-helix at the N-terminus and a 3_{10}-helix at the C-terminus.[17,70,71] To further investigate the stability of the conformation in different solvents, the **T^{N}-Zrv-T^{C}** analog, with two TEMPO spin labels attached at both the N- and C-ends, was studied by PELDOR in frozen solutions of MeOH, MeOH/toluene, and MeOH/CHCl$_3$.[48,49] It was shown that in MeOH the main maximum of the distribution functions is located at a distance of *ca*. 3.2 nm (Table I). This distance appears to be only slightly dependent on the solvent composition, but the distribution function was observed to narrow after addition of either CHCl$_3$ or toluene to MeOH. This effect was rationalized in terms of a decreased mobility of both sequence termini. By molecular dynamics simulations it was shown that the conformation corresponding to the predominant PELDOR distance agrees well with the mixed α/3_{10}-helix previously determined by NMR. However, when toluene was added to the MeOH solution (to further increase the hydrophobicity of the environment of this membrane-active peptide) the distribution function gives also rise to a minor fraction (7-8%) with a distance of 4.2 nm. Most likely, this distance corresponds to the more elongated 2.2_7-helix structure.

Alamethicin F50/5

To determine the conformation of alamethicin F50/5, a long (19-amino acid residue) peptaibol,[72] the double spin-labeled analog **Alm^{1,16}** was investigated in frozen solutions of MeOH and MeOH/toluene (1:4) (Table I).[65] The r_{max} ~ 2.1 nm was found in excellent agreement with the average distances calculated from a set of five models, which are derived from the almost completely α-helical crystal structures.[16,73] Such distances between labels correspond to the α-helix conformation, at least for the segment 1-16 of this peptide. Compared to the previous results

obtained for trichogin, the conformation of alamethicin is remarkably stable. In particular, it does not depend on the polarity of the medium (MeOH or MeOH/toluene).

Covalent Dimer of Trichogin GA IV

It is the longest (22-amino acid residue) peptaibol examined by PELDOR, designed and synthesized explicitly to this purpose. In Figure 7B the distance distribution functions obtained for the double spin-labeled peptide **D-Tri[1,19]** in MeOH/toluene mixtures can serve as an example showing solvent effects on self-aggregation and the concomitant alteration of the secondary structure.[66,67] In pure MeOH, oscillations of the PELDOR time trace are weak and the poorly resolved doublet has a total width of nearly 2 nm (Table I). Addition of toluene leads to an increase of the oscillation amplitude and the function $F(r)$ exhibits two pronounced maxima corresponding to distances of 2.8 and 3.2 nm (related to α-helix and 3_{10}-helix conformations, respectively) (Figure 7B). In pure toluene, the PELDOR time trace is strongly modulated and the main maximum corresponds to α-helical aggregated molecules.

SPIN LABELED PEPTAIBOLS: QUATERNARY STRUCTURES

1.STUDIES IN FROZEN GLASSY SOLUTIONS

Data for the quaternary structures of spin-labeled peptaibols in solvent mixtures of low polarity obtained by PELDOR spectroscopy are discussed in this section.

Table II Quaternary Structures of Mono Spin-labeled Peptaibols in Solvent Mixtures of Low Polarity

Peptaibol Analog	Label Positions	Solvent	N^a	Packing Mode	Ref
O-Tri	1, or 4, or 8	CHCl$_3$/toluene	4	antiparallel	60,74
Tyl	3 or 13	MeOH/toluene	2	head-to-head^b	61,62
Hep	2 or 14	MeOH/toluene	2	head-to-tail/head-to-head^b	61,62
Zrv-T^C	C-term	MeOH/toluene	2	antiparallel	48,49
Alm	1, or 8, or 16	CHCl$_3$/toluene	8	parallel dimer of a linear tetramer	75,76
D-Tri	1, 19	CHCl$_3$/toluene	2	antiparallel	66,67

^{a} Oligomeric number. ^{b}Probably a mixture of aggregates of different types.

Trichogin GA IV

As we have seen earlier in the text, transition from polar to nonpolar solvents leads to change in the conformation and concomitant aggregation.[74] In the latter media, for both **F-Tri[4]** and **O-Tri[1]** mono spin-labeled analogs, the fast drop of the PELDOR time traces at low T is followed by a slow decay modulated by the dipolar interaction (Figure 8, curves 1 and 2). Addition of the polar solvent ethanol (EtOH) to the same samples causes a change to the exponential functions (Figure 8, curves 3 and 4), indicating disruption of the aggregates. For both **F-Tri[4]** and **O-Tri[1]**, the number of spin labels in the aggregates was found to be $N = 4 \pm 0.3$ and the intermolecular distances between spin labels within the aggregates are $r = 2.35$ nm and $r = 2.60$ nm, respectively. Analogous peculiarities of the aggregation phenomena were also shown for other frozen glassy solutions (CHCl$_3$/toluene, CHCl$_3$/decalin, CCl$_4$/toluene, dichloroethane/toluene).
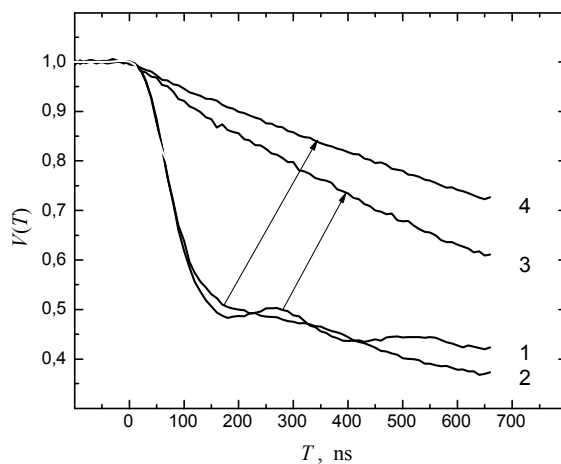

FIGURE 8 $V(T)$ time traces for mono spin-labeled **F-Tri[4]** and **O-Tri[1]** in CHCl$_3$/toluene (curves 1 and 2, respectively) and the effect on $V(T)$ upon addition of EtOH (curves 3 and 4, respectively). All measurements were performed at 77K.

In particular, it was demonstrated that the type of quaternary structures depends on solvent properties: r_{max} between 2.3 and 3.3 nm, N between 3.1 and 4.3.[77] Similar data were obtained for double spin-labeled trichogin analogs.[60] All these experimental results are consistent with the molecular model presented in Figure 9.[74] This tetrameric arrangement in nonpolar media was constructed from **O-Tri[4,8]** 3_{10}-helices. The four helices are formed by two dimers, mutually oriented in an antiparallel disposition. In this vesicular system the polar main-chain groups point to the interior of the cavity and the apolar chains to the exterior of the cluster.
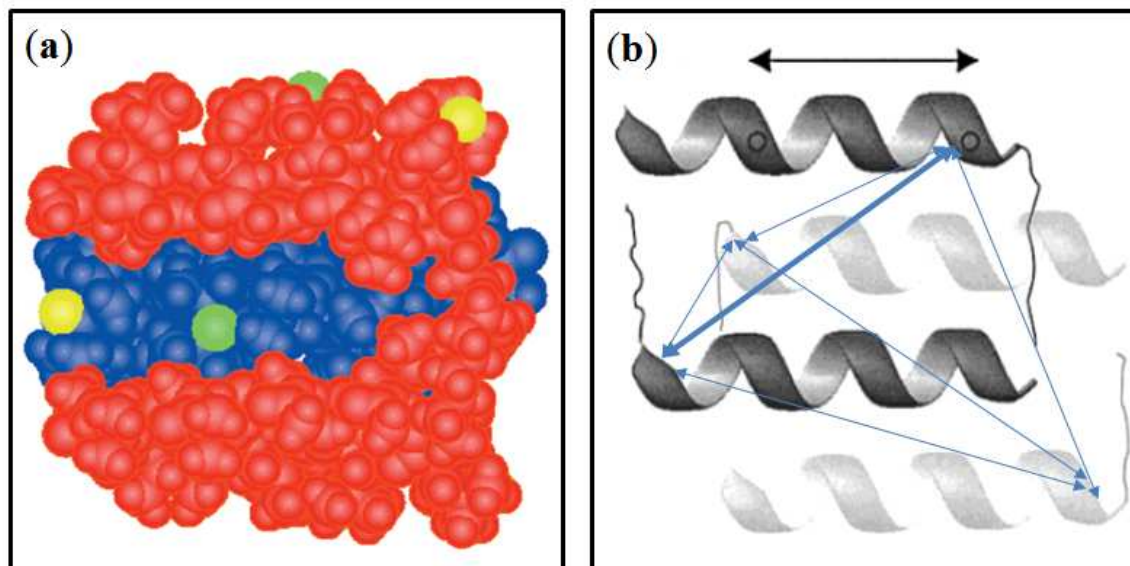
FIGURE 9 (a) A space-filling molecular model of the quaternary structure of the aggregate of the double spin-labeled **O-Tri**[1,4] analog in nonpolar media. **(b)** A ribbon drawing of the supramolecular assembly of one double spin-labeled (**O-Tri**[1,4]) and three unlabeled (**O-Tri**) peptide chains. For clarity, the distances are only shown for the TOAC[1] positions.

These results were corroborated by our cw EPR data.[78,79] At room temperature in the CHCl$_3$/toluene solvent mixture two different sets of signals were observed which were attributed to the concomitant presence of monomers and aggregates. A two-step aggregation mechanism was proposed: dimerization of the peptide molecules, followed by aggregation of the dimers assembling to four peptide molecules per aggregate. The equilibrium constants were estimated for both steps. Further analysis of the line widths allowed us to assess the rotational mobility of both the aggregates and the monomers. The number of peptide molecules per aggregate was estimated to be $N \approx 4$. The intermolecular distances between the labels in aggregates of **O-Tri**[8] and **O-Tri**[1] were determined to be about 0.1 and 1.6 nm, respectively. These findings agree well with a helix bundle where the helices are oriented in an antiparallel fashion.

In a previous paper,[28] cw EPR spectra were recorded at $g = 4.0$ and at half-field. It was reported that spin-labeled trichogin GA IV analogs exist in a mixed $\alpha/3_{10}$-helical conformation (in equilibrium with some C-terminally unfolded conformers). The same type of mixed helical conformation was authenticated in the crystal state by X-ray diffraction analyses for natural trichogin GA IV[18] and two **Tri**[4,8] analogs.[19]

Tylopeptin B and Heptaibin

Tylopeptin B was studied with spin labels incorporated at position 3, 8 or 13,[61,62] while heptaibin analogs were labeled at position 2 or 14.[61,62] Peptide aggregation of tylopeptin B was

investigated in weakly polar MeOH/toluene environments. Based on the concentration dependencies of the modulation depth, the number of peptide molecules in the aggregates of this peptaibol was estimated ranging from 2 to 3. Dimer formation was suggested to be the prevailing mode of self-association with the molecules arranged in a head-to-head fashion. The width of the distance spectrum, Δ, of **Tyl^{13}** appears much broader than that of the analog **Tyl^{3}**, the latter with the label at the N-terminus. It might be possible that the C-termini of the molecules are more mobile than the N-termini. For heptaibin, two forms of dimerization (head-to-head and head-to-tail) were found. In addition to dimers, aggregates may contain 3 or 4 peptide molecules, as indicated by broad lines in the distance spectra.

Zervamicin II A

Aggregation of mono spin-labeled zervamicin **Zrv-T^{C}** molecules was studied in toluene/MeOH mixtures (8.5-16% in MeOH).[48,49] In this case, the PELDOR time trace does not show oscillations, but rather a fast decay followed by attainment of a constant limiting value of V_p. This type of trace is characteristic of a group of electron spins generated by aggregation of N spin labeled molecules. One can estimate the effective distance r_{eff} between spins in the group from the characteristic time of the initial $V(T)$ trace decay $T^* = r^3_{eff}/D$ (see Eq. 8 and the text below). It was found that r_{eff} varies between 2.5 and 3.5 nm, dependent on solvent. From the NMR experiments, the length of the helical zervamicin molecule in solution is 2.56 nm.[17] Thus, the intermolecular distance between the C-terminally located spin labels of **Zrv-T^{C}** within the aggregate is consistent with a model of antiparallelly oriented peptaibol molecules. Moreover, the N value calculated from relation (Eq. 9) depends on the composition of the solvent mixture: $N_{max} = 2$ contains at least 44-67% of **Zrv-T^{C}** molecules. Unfortunately at present, there is a serious lack of 3D-structural information on zervamicin which prevents the construction of a reliable molecular model for the aggregate of this peptaibol.

Alamethicin F50/5

Site-specific mono spin-labeled **Alm** analogs were investigated by cw ESR and PELDOR techniques.[75,76] Analysis of the $F(r)$ functions (Figure 10a) obtained for peptides spin-labeled at different positions in CHCl$_3$/toluene (1:1) in the concentration range 10^{-3}-10^{-4} mol/l showed the following results. All three $F(r)$ functions have similar shapes and nearly the same parameters: (i) a main, sharp maximum at 3.18 (**Alm^{1}**), 3.24 (**Alm^{8}**), and 3.06 nm (**Alm^{16}**), and a broad maximum at about 7 nm. Nearly 30% of the spin labels exhibit short distances and the remaining species (70%)

are in the region of 7 nm. From the analysis of the $V(T)_{intra}$ and $F(r)$ parameters, it follows that in the aggregate the N value may vary from 6 to 8.

To obtain a more reliable N value, the cw EPR line shapes of these peptides were examined in chloroform/toluene at room temperature. From the correlation times of rotational mobility,[80] the N value was estimated to be $N= 6.8 \pm 2.5$. Thus, combining PELDOR and cw EPR results, this number varies between $6 \leq N \leq 9$. Based on the data obtained, a model for the **Alm** aggregate was proposed as two linearly aligned tetramers (Figure 10c).
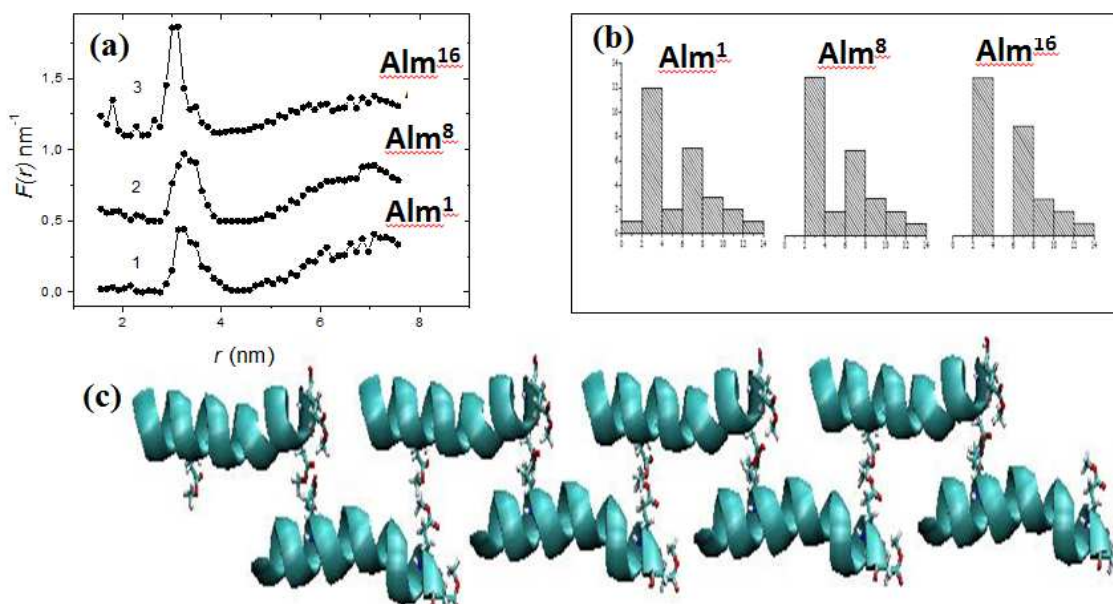
FIGURE 10 (a) Distance spectra $F(r)$ for mono spin-labeled **Alm**[1], **Alm**[8], and **Alm**[16] aggregates in $CHCl_3$/toluene (1:1) at 77 K. For convenience of comparison, curves 2 and 3 are shifted upwards by 0.5 and 1.1, respectively. **(b)** Histograms showing the number and distribution of distances found for **Alm**[1], **Alm**[8], and **Alm**[16] situated in the octamer model (MD calculations). The total number of distances determined for each aggregate is 28. **(c)** Molecular model of the supramolecular aggregate of the **Alm** octamer composed of two parallel main-chains, each built from four head-to-tail associated molecules.

To verify the model proposed, detailed MD calculations were carried out. From the experimental findings it follows that the minimum peptide···peptide interaction energy is attained at a distance of 3.3 nm for those molecular conformations in which the Glu γ-ester groups at positions 7, 18, and 19 in both peptides interact as dipoles with antiparallel orientations, thus forming seven polar clusters along the alamethicin aggregate. Figure 10b shows that the histograms of the distribution over the number of different distances for the model proposed are in qualitative agreement with the experimental functions $F(r)$ for the mono spin-labeled **Alm**[1], **Alm**[8], and **Alm**[16].

1
2
3
4
5
6
7
8
9
10
11
12
13
14
15
16
17
18
19
20
21
22
23
24
25
26
27
28
29
30
31
32
33
34
35
36
37
38
39
40
41
42
43
44
45
46
47
48
49
50
51
52
53
54
55
56
57
58
59
60

Covalent Dimer of Trichogin GA IV

It is the longest peptaibol ($n = 22$) that was studied by PELDOR.[66,67] The aggregate of the mono spin-labeled peptide **D-Tri**[1] showed $N\sim2$ (based on the V_p value) and a distance between the spin labels of 3.4 nm. This finding implies an antiparallel orientation of the molecules in the aggregate. When constructing a model, one should take the electrical dipole moment of the peptide helix into account. In particular, the estimated total dipole moment of the α-helix in **D-Tri**[1] equals to 77.0 D and is aligned to the helix axis. The distance between the α-helices (0.8 nm) is determined by steric factors only. The 3D-structural model for the **D-Tri**[1] peptide aggregates is shown in Figure 11.
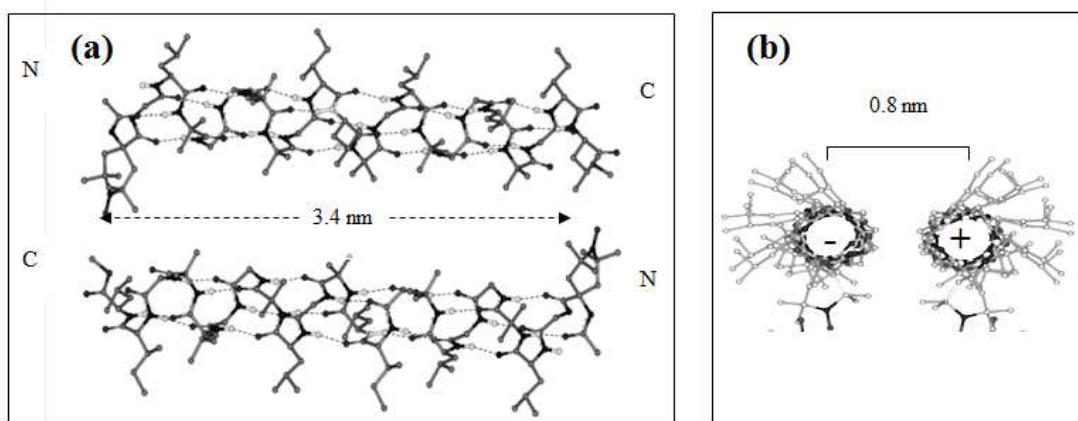

FIGURE 11 (**a**) 3D-Structural model of the **D-Tri**[1] aggregate: molecules with an antiparallel orientation and a label⋯label distance in the dimer of 3.4 nm and (**b**) a view along the axes of the α-helices. The centers of the two helices are separated by about 0.8 nm.

2. STUDIES IN MODEL MEMBRANE SYSTEMS

Trichogin GA IV

Despite the limited length of its main chain, trichogin GA IV exhibits remarkable membrane-modifying properties.[12,13,15] To elucidate the mechanism by which this short peptide changes membrane permeability, detailed information was needed about its aggregation state in the membrane of liposomes. The experimental distribution function depicted in Figure 12 exhibits a maximum near 2.5 nm and a half width of 1.4 nm. This latter parameter indicates a broad distance distribution. From such a distance spectrum, which could indicate the presence of aggregates of different types, we calculated a value for N of 2.1 ± 0.1. Thus, at a (local) peptide concentration of 5 mol % in DPPC (1,2-dipalmitoyl-*sn*-glycero-3-phosphocholine) membranes, the aggregates are

mostly formed by pairs of trichogin molecules. It is worth noting that for the spin-labeled trichogin in different membrane-mimicking solvent systems, the aggregate number was found to vary between $N = 1$ (monomer, in the polar solvent EtOH) and $N = 4.3$ (in the almost apolar dichloroethane/toluene mixture). At much lower total concentrations, experiments with fluorescent trichogin analogs and large unilamellar vesicles (LUVs) of egg phosphatidyl choline (ePC) in the presence of cholesterol showed a lower limit of the number of molecules per aggregate, $N = 2.3$.[81] At about the same total concentration, an ion conduction experiment with unlabeled trichogin bound to ePC LUVs in the absence of cholesterol demonstrated that 3 to 4 molecules are involved in the rate-limiting step.[82]
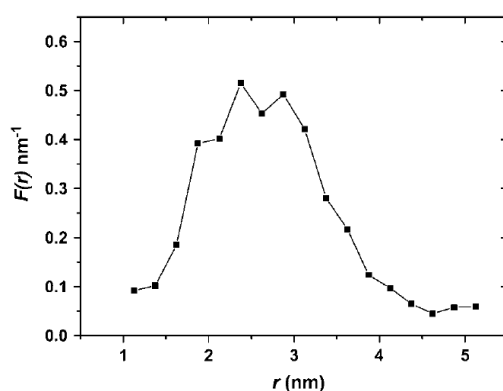
FIGURE 12 Distance distribution function F(r) between spin labels of **F-Tri[1]** aggregates in DPPC lipid bilayers.

On the other hand, another PELDOR study of **O-Tri[4]** in ePC vesicles showed that, over the range of peptide to lipid concentration 0.5–2.2 mol %, trichogin molecules are homogeneously distributed at the inner and outer membranes,[83,84] whereas upon addition of cholesterol the distribution was found to be inhomogeneous. Therefore, the presence of cholesterol is clearly promoting formation of thermodynamically stable aggregates. However, we cannot exclude the possibility that, under the conditions used for ion conduction experiments, larger oligomeric species might be penetrating the hydrophobic core of the lipid bilayer.

As already stated earlier in the text, inspection of crystallographic data for trichogin GA IV highlights a mixed 3_{10}-/α-helix structure for the peptide backbone.[18,19] Since the α- and 3_{10}-helices exhibit different main-chain lengths, PELDOR was used to determine the conformation for its membrane-bound state.[66,67,83-85] Thus, when two TOAC residues are concomitantly incorporated at the ends of the peptaibol, information about its conformation can be obtained from the intramolecular distance between the nitroxide labels. In Figure 13a, the distance distribution

function is reported for the double spin-labeled **F-Tri^{1,8}** in eggPC membranes[83] (eggPC membranes are composed of a mixture of saturated and unsaturated lipids of different lengths). Two main maxima are shown at distances of 1.25 and 1.77 nm, which correspond to α- and 3_{10}-helical conformations, respectively. Apparently, the peptaibol appears as a mixture of conformations, with the α-helix being more densely populated.

In Figure 13b, the distance distribution function is described for **O-Tri^{1,8}** in membranes composed of saturated DPPC lipids.[85] Under these conditions, the observed intramolecular distances also correspond to a mixture of α- and 3_{10}-helix populations, but in this case the 3_{10}-helix is favored. Since in both eggPC and DPPC membranes the lipopeptide molecules were found mono-molecularly associated to the PC head-group regions of the membranes,[85] the different ratios of helix populations observed in the two experiments cannot be caused by a different molecular environment (*e.g.*, polar head group *vs*. hydrophobic core of the membrane), or a different aggregation state. It is worth noting that these trichogin analogs are capped by two different groups at the N-termini of the peptides, *i.e.*, the Fmoc group (Figure 13a) and the Oct group (Figure 13b). The Fmoc group is characterized by a fused, rigid aromatic moiety (that is linked *via* a carbamate functional group to the N-terminus), while the Oct group exhibits a long and very flexible hydrocarbon chain (linked to the N-terminus *via* an amide function). Although stabilization of a peptide helix by capping of its N-terminus is a well-known phenomenon,[86] the physical basis for the observed different helix populations shown in Figure 13 remains unclear. Probably, the more rigid, aromatic N-capping group is stabilizing the α-helix better than the more flexible, aliphatic group.
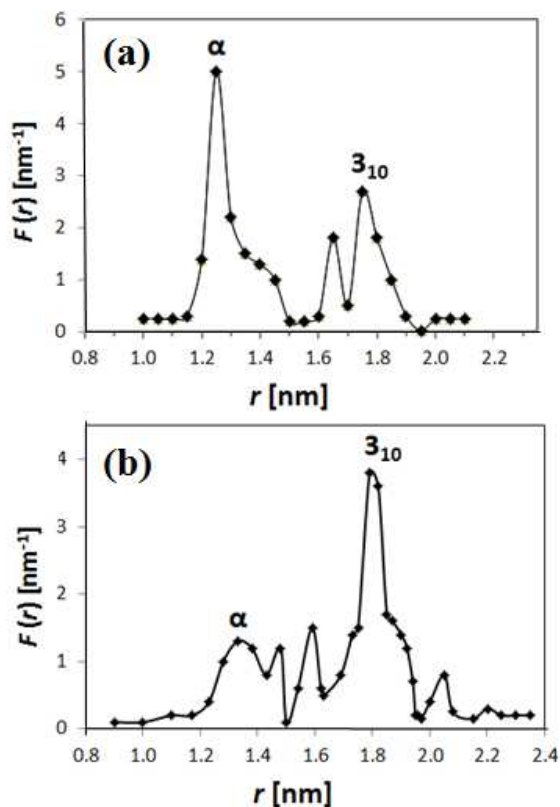
FIGURE 13 Distance distribution functions obtained for **F-Tri[1,8]** in eggPC (**a**) and for **O-Tri[1,8]** in DPPC membranes (**b**).

As mentioned above, 3_{10}-helices are considered kinetic intermediates in the mechanism of folding of α-helices of proteins.[55,56] For peptides shorter than heptamers, the 3_{10}-helix tends to prevail.[23,24,50,57] This effect can be understood from the analysis of the diverging H-bond forming patterns, since these two helices differ for the relative positions of the C=O and N-H groups involved in H-bond formation ($i \leftarrow i+3$ and $i \leftarrow i+4$ in 3_{10}- and α-helices, respectively). Also the environment of the molecules is an important determinant for conformational stabilization. For instance, solvent titration studies of the covalently linked head-to-tail (C-to-N) dimer of trichogin GA IV (**D-Tri**) showed a strong dependence of the conformational behavior on both solvent polarity and aggregation state.[66,67] Therefore, it seems reasonable to assume that the position of the conformational equilibrium will shift following the penetration of the lipopeptide from the polar head group into the core of the membrane. In the case of a hydrophobic environment, the equilibrium would be expected to increase the extent of the α-helical conformation. However, if the channel-forming peptide remains associated with bulk water, as we have shown for **F-Tri[1,8]** in eggPC/cholesterol,[87] then the 3_{10}-helix will be favored.

The N^α-blocking, fatty acyl moiety was also demonstrated to play a major role in the antibiotic properties of **O-Tri**.[14] At least six carbon atoms of the aliphatic chain are required for significant membrane and antibiotic activities, while the C2 and C16 analogs of the lipidic chain were found to be inactive. The absence of activities observed for the C2- and C16-acylated peptaibol analogs is likely explained by a lack of hydrophobicity for the former and a too slow diffusion rate to reach the membrane for the latter. Interestingly, a similar N^α-acyl group-dependent trend was also found for the hemolytic (toxic) activities of the trichogin GA IV analogs investigated at higher peptide concentrations. Note that the slow diffusion of the C16-analog might be caused by a slow dissolution rate of the membrane surface-aggregated lipopeptide, as we described above for the double spin-labeled C8-acylated analog (**O-Tri**[1,8]).

A considerable body of evidence has been accumulated to support the view that, at low peptide concentration where trichogin GA IV is known to exhibit antibiotic activity, the peptide helix is bound parallel to the membrane surface. However, a comparison between the antibiotic activities of natural trichogin GA IV and its covalently linked C-to-N dimer (**D-Tri**) against S. *aureus* bacteria showed a significantly higher potency for the latter, even at extremely low peptide concentration.[14,66,67] The increased antibiotic activity reported for **D-Tri** might be possibly correlated with the proposed model of a transmembrane-oriented and non-covalently bound dimer of trichogin GA IV, which was based on experiments recorded at higher peptide concentrations. Therefore, the trichogin GA IV-induced transport of ions through the nonpolar part of the membrane is probably realized by insertion into the bacterial membrane activated by the natural voltage potential.[82,88,89]

Alamethicin F50/5

Pulsed EPR spectroscopies were also exploited to study the self-assembled superstructure of the **Alm** molecules in vesicular membranes (at peptide to lipid molar ratios in the range 1:70–1:200).[90-93] From the magnetic dipole⋯dipole interactions between the nitroxides of the mono spin-labeled constituents and the PELDOR time trace measured at 77 K, intermolecular distance distribution functions were obtained and the number of aggregated molecules ($N \approx 4$) was estimated. All distance distribution functions exhibit a similar maximum at 2.3 nm. In contrast to **Alm**[16], for **Alm**[1] and **Alm**[8] additional maxima were recorded at 3.2 and ≈ 5.2 nm (Figure 14).
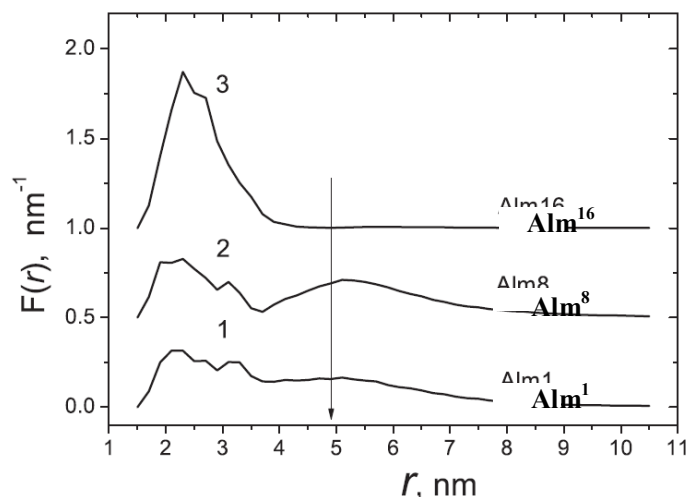
FIGURE 14 Distance distribution functions F(r) between TOAC spin-labels for **Alm** analogs in membranes of frozen ePC vesicles. For clarity, curves 2 and 3 are shifted upward by 0.5 and 1.0, respectively. The distance distributions are obtained from the experimental V_{INTRA} decays by the Tikhonov regularization method. The shape of $F(r)$ at distances longer than that indicated by the arrow is not real and can be used only for estimation of the area under the broad line.

An important observation of the distance distribution curves is that, independent of the spin label position, similar distance maxima are seen (~2.3 nm). This finding agrees well with a simple model of parallel alignment of a face-to-face type of helix···helix association with the polar groups oriented to the inside and the spin labels located at the outside of the superstructure, but it disagrees with an antiparallel orientation. In the latter case, the computed distance between the TOAC[16] labels would be 3.4 nm, which is at the extreme side of the experimental distance distribution curve 3. To gain insight into the helix···helix interactions in more detail, a molecular modeling study was carried out. In this investigation a set of distance restraints was used that was taken from the intermolecular PELDOR distances between the TOAC labels. For convenience, but differently from the actual experiments, each peptide molecule was labeled threefold (at positions 1, 8, and 16). In Figure 15, the computed gas-phase, energy-minimized peptide complex is built from four parallel, but slightly tilted, α-helices. A more in-depth examination of the aggregate structure shows that all peptide helices are slightly perturbed due to the missing H-bond at the helix breaking tetrapeptide region from Gly[11] to Pro[14]. It is worth noting that bending of the peptide helix was also found in a ^{1}H-NMR study of micelle-associated **Alm**.[94]
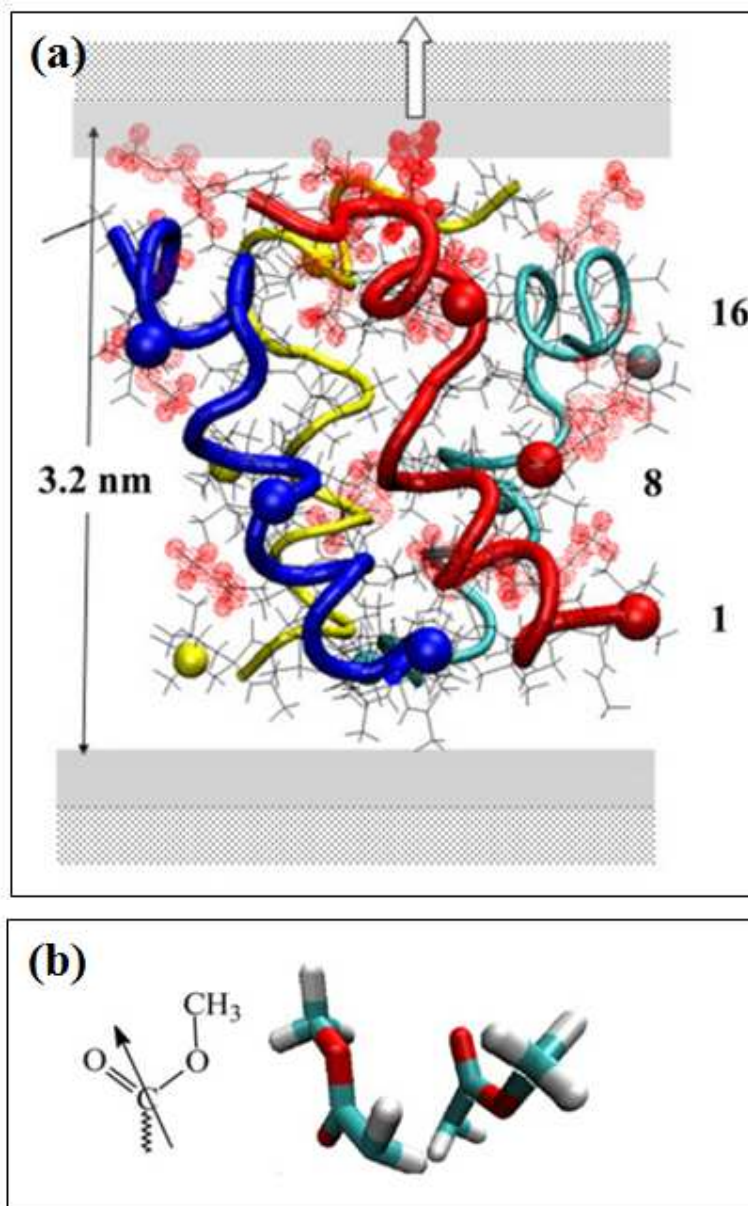
FIGURE 15 (a) Energy-minimized model of the supramolecular, threefold labeled **Alm** tetramer, which is based on the short 2.3 nm PELDOR distance between the exocyclic oxygen atoms of the TOAC[1], TOAC[8], and TOAC[16] residues. The spatial positions of the oxygen atoms are indicated by balls, with the TOAC[1] labels shown at the bottom of the Figure. For clarity, but differently from our experiments, each peptide is threefold labeled. The side view of the tube model shows the spatial arrangement of four parallelly aligned α-helical peptide chains. In each helix the 3D-structure is bent at the Leu[12]-Aib[13] level due to the missing H-bond between the carbonyl oxygen of Gly[11] and the tertiary nitrogen atom of Pro[14]. **(b)** Mutual positions of the -COOMe groups (for clarity, only two of them are shown). Electrical dipole···dipole interactions between the ester groups stabilize the parallel orientation of the helix bundle and are also key determinants to anchor the aggregate to the polar region of the membrane.

To confirm whether the α-helical conformation of the associated peptide molecules of the supramolecular model illustrated in Figure 15 is correct, the non-restrained intramolecular distances between the TOAC[1] and TOAC[16] residues of the model were compared with the corresponding

experimental distance determined previously by PELDOR for ePC membrane-bound aggregates of the double spin-labeled **Alm[1,16]** analog.[65] In the latter study, the average of the intramolecular distance between these two labels was found to be 2.1 nm (with a deviation of 0.5 nm for each of the peptide molecules of the ePC-bound aggregate), independent of the peptide to lipid ratio (1:50 or 1:200). The comparison indeed shows that the theoretical distance matches the experimental one (within experimental error), despite the perturbation induced by the Gly[11]-to-Pro[14] sequence. Thus, the conformation of the membrane-bound peptides is likely to be α-helical. Further inspection of the model shows that the intermolecular distances between the exocyclic oxygen atoms of the TOAC residues (1.8 nm) fall within the first peak of the PELDOR experiments, but not at the maximum of 2.3 nm. Clearly, our minimalist, gas-phase model is, at least partially, flawed here (*vide infra*). Next, the model structure was oriented with respect to the membrane normal by adjusting the parallelly aligned N-terminal helices to tilt angles of 15° (blue and red colored chains), 13° (cyan), and 8° (yellow), in a similar manner as it was found in EPR and solid-state NMR analyses of **Alm**.[95,96] According to Figure 15b, the lengths of the blue, red, and yellow colored transmembrane helices (≈ 3.2 nm) are likely matching the hydrophobic thickness of the ePC membrane (≈ 3.5 nm), in view of the uncertainty of the applied conversion factors to calculate the thickness of the membrane[97,98] and the possibility of peptide-induced membrane thinning effects.[99] The C-terminus of the cyan colored chain, however, is immersed more deeply into the hydrophobic region of the membrane.

Finally, the positions of the polar Glu(OMe)[7,18,19] residues of **Alm** with respect to the different hydrophobic, polar, and zwitterionic choline regions of the membrane might be of interest in view of their possible role in the closed (non-conducting) state of the **Alm** channel. In Figure 15b these positions are indicated by dotted circles, schematically suggesting their uncertainties due to the flexibilities of the long γ-ester side chains. Four out of a total of eight of the C-terminal residues are located in or nearby the polar lipid ester region of the membrane, whereas the remaining residues are buried more deeply. Figure 15a shows that the two carbonyl esters of the Glu(OMe)[18] side chains of the red and cyan molecules are mutually located at a close distance (0.36 nm). It should be noted that in our previous investigation of aggregates of **Alm[1]**, **Alm[8]**, and **Alm[16]** in hydrophobic solvents (to mimic the hydrophobic interior of the membrane), the electric dipole···dipole interactions between the γ-ester groups were found to be the key determinant to stabilize the peptide complex. Thus, it seems that the association of the C-termini of the peptide cluster in the ePC membrane is stabilized in a similar manner. One might also speculate about the role of the γ-ester groups of the Glu(OMe)[19] residues to anchor the aggregate to the polar region of the membrane by dipole···dipole interaction with the surrounding lipid ester groups.

3. STUDIES IN WHOLE CELL MEMBRANES

Trichogin GA IV

Spherical cells of the Gram-positive bacterium *Micrococcus luteus* were selected to investigate the structural features of the bound trichogin GA IV antibiotic molecules. An advantage to use a Gram-positive microorganism is its rather simple architecture, *i.e.* a single lipid bilayer surrounded by a thick peptidoglycan cell wall. The PELDOR technique was used to investigate the dipole···dipole phase relaxation of the mono spin-labeled peptide **O-Tri[4]** in the cell membrane of *Micrococcus luteus*.[43] The particular aim of this work was to examine the mutual, homogeneous or nonhomogeneous, distribution, and the occurrance of aggregates of the lipopeptaibol molecules in the bulk membrane or on its surface.

The local concentration of the spin labels in the cell suspension was estimated by comparing the PELDOR time traces measured for different spin concentrations in both EtOH and the cell suspension. The value of the local concentration of **O-Tri[4]** in the cell was found to be 2.7 x 10^{-3}, which corresponds to a mean distance between spin labels of ~8 nm. This value is of the same order as the thickness of the cell membrane (7 nm, including membrane proteins bulging out of the lipid bilayer). This observation demonstrates that this peptide is capable to diffuse through the peptidoglycan cell wall of 20 nm thickness and to target the lipid membrane. No fast PELDOR decays were observed, as would be expected for peptaibol aggregates. This finding indicates a mono-molecular state of membrane bound **O-Tri[4]**. This observation agrees with the PELDOR experiment of the same **Tri** analog in liposomes (*vide supra*).
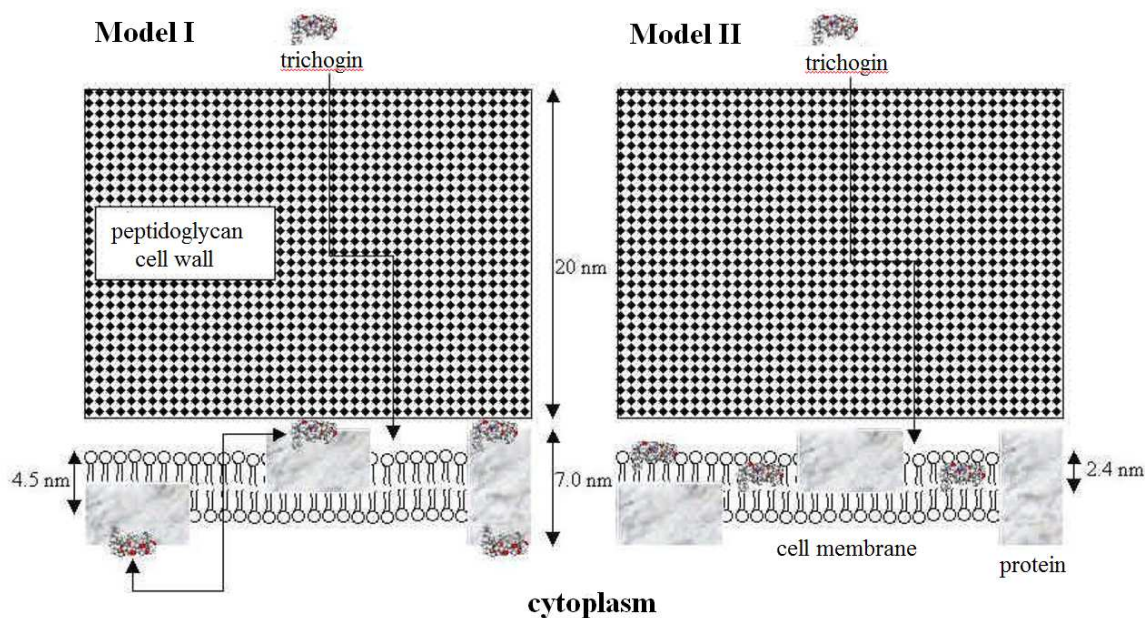
FIGURE 16 Two different binding modes of trichogin GA IV to *Micrococcus luteus* cells. Model I: trichogin molecules bound to bulging membrane proteins at both sides of the double layer. Model II: trichogin molecules bound to the periplasmic side of the membrane and distributed into a layer of 2.4 nm thickness.

Based on further analysis of the experimental data, two different models were proposed: (i) a random distribution on both inner and outer surfaces of the membrane at a distance between the surfaces of 7 nm, and (ii) a random distribution in a *ca.* 2.4 nm thick layer below the outer surface (Figure 16).

In conclusion, the data obtained for the phase relaxation of spin labels for **O-Tri⁴** bound to frozen *Micrococcus luteus* cells exclude the possibility of membrane bound aggregates. The main target of the peptaibol after penetration of the porous cell wall is the phospholipid cytosolic membrane. Whether the peptide molecules are bound to phospholipids (cardiolipin and phosphatidyl glycerol are the major constituents[100,101]) or to membrane proteins (49 % *w/w* of the membrane[102]) is not clear yet and will be the subject of further studies from our groups.

SUMMARY AND OUTLOOK

The large body of experimental data presented in this review article well justifies our assumption that PELDOR spectroscopy technique has recently further expanded its field of applications. In particular, here we have shown its use to reach two purposes: (i) efficiently measuring distances between synthetically, site-directed, paramagnetic labels in the scale of distances between 1.5 and 7.5 nm in peptides with good accuracy, and (ii) unraveling the organization of peptide supramolecular self-assemblies and mechanisms of interaction with model and biologically relevant (even whole cell) membranes. The specific subject of this ongoing, joint effort among our research groups is the class of peptaibols. These emerging peptide molecules are endowed with potentially interesting antibiotic activity, associated with their marked ability to disrupt the membrane 3D-structure. This property is generated in turn by their stable α-/3_{10}-helical conformations (induced by the massive occurrence of Aib residues in their sequences), accompanied by their intriguing combination of apolar (side chains and terminal blocking groups) and polar (poly-amide backbone) properties.

In particular, we have investigated the preferred secondary structures of double nitroxide spin-labeled analogs of six, naturally-occurring, peptaibols: trichogin GA IV, tylopeptin B, heptaibin, ampullosporin A, zervamicin II A, and alamethicin F50/5, together with the artificially-planned trichogin GA IV covalent dimer. These compounds are good representatives of the whole class of peptaibols, as they differ in: (i) main-chain length, (ii) percentage of helicogenic Aib, and (iii) amount of helix-interrupting Pro (or Hyp) residues in their sequence. Solvents and solvent mixtures of different polarities as membrane-mimicking environments, and model membranes as well, were examined. Different helical structures of diverging length were identified and their relative extent shown to be sensitive to chemical structure and surrounding media (molecular spring effect). The myriad of naturally-occurring peptaibols of different characteristics sequenced in the last few years, some of them exhibiting surprising properties of biomedical interest, is still awaiting to be explored by available spectroscopies. Among them, PELDOR application to appropriately planned and synthesized double nitroxide spin-labeled analogs will certainly prove to be an essential source of useful information.

More useful to our understanding of the biophysically relevant behavior of peptaibols is the variety of evidence accumulated on their modes of self-assembly (quaternary structures) in membrane-mimicking solvent mixtures. Our findings indicate that self-assemblies of **O-Tri**, **D-Tri**, and **Zrv-T^C** molecules, dictated by electric dipole$\cdots$dipole (main chain-to-main chain) interactions, stabilize an antiparallel superstructure of dimer/tetramer associations. Moreover, **Tyl**

and **Hep** tend to exist as mixtures of different types of aggregates, but with the head-to-head dimer formation as the principal mode of self-aggregation. Finally, our model of **Alm** self-assembly implies the onset of an octamer composed of two parallel main-chain systems, each generated by four head-to-tail associated molecules.

In the last part of our paper, we presented our results on the quaternary structures of (mostly single nitroxide spin-labeled) peptaibols induced by model membrane systems and whole cell membranes as well. To date, only preliminary studies (and limited to two peptaibols, namely **Tri** and **Alm**), were performed. Also, exclusively the former compound was investigated in the presence of whole cell membranes. In lipid membrane model systems, the quaternary structure of trichogin molecules is not well defined yet. In whole cell membranes, these molecules seem to essentially remain in the monomeric state. Conversely, our PELDOR data on **Alm** analogs were found complementary to the NMR findings. The observed parallel manner of association is likely to be governed by the interactions of their polar, C-terminal Glu γ-methyl esters with the polar head of the lipid bilayer. This behavior is in contrast with the antiparallel arrangement of **Alm** molecules seen in solvents of low polarity, where the self-aggregates are most probably stabilized by dipole···dipole interactions.

In any case, it is clear that ample scientific space is still open to collaborations between biophysicists and peptide chemists aiming at deeply elucidating the aggregation modes of these two and other peptaibols with different conformational properties in the presence of membrane environments.

Acknowledgements

REFERENCES

1. Milov, A.D.; Salikhov, K.M.; Schirov, M.D. Solid State Phys (Russian) 1981, 23, 975-982.

2. Pannier, M.; Veit, S.; Godt, A.; Jeschke, G.; Spiess, H.W. J Magn Reson 2000, 142, 331-340.

3. Tsvetkov, Yu.D.; Milov, A.D.; Maryasov, A.G. Russian Chem Rev 2008, 77, 487-520.

4. Tsvetkov, Yu. D. J Struct Chem 2013, 54, Suppl. 1, S42-S72.

5. Dzuba, S.A. Russian Chem Rev 2007, 76, 699-713.

6. Schiemann, O. Methods in Enzymology 2009, 469, 329-351.

7. Reginsson, G.W.; Schiemann, O. Biochem Soc Trans 2011, 39, 128-139.

8. Reginsson, G.W.; Schiemann, O. Biochem J 2011, 434, 353-363.

9. Jeschke, G.; Sajid, M.; Schulte, M.; Ramezanian, N.; Volkov, A.; Zimmermann, H.; Godt, A. J Am Chem Soc 2010, 132, 10107-10117.

10. Pornsuwan, S.; Schafmeister, C.E.; Saxena, S. J Phys Chem C 2008, 112, 1377-1384.

11. Fedorova, O.S.; Tsvetkov, Yu.D. Acta Naturae 2013, 5, 8-14.

12. Toniolo, C.; Crisma, M.; Formaggio, F.; Peggion, C.; Epand, R.F.; Epand, R.M. Cell Mol Life Sci 2001, 58, 1179-1188.

13. Peggion, C.; Formaggio, F.; Crisma, M.; Epand, R.F.; Epand, R.M.; Toniolo, C. J Pept Sci 2003, 9, 679-689.

14. Toniolo, C.; Crisma, M.; Formaggio, F.; Peggion, C.; Monaco, V.; Goulard, C.; Rebuffat, S.; Bodo, B. J Am Chem Soc 1996, 118, 4952-4958.

15. Rebuffat, S.; Goulard, C.; Bodo, B.; Roquebert, M.-F. Recent Res Devel Org Bioorg Chem 1999, 3, 65-91.

16. Fox, R.O., Jr., Richards, F.M. Nature (London) 1982, 300, 325-330.

17. Karle, I.L.; Flippen-Anderson, J.; Sukumar, M.; Balaram, P. Proc Natl Acad Sci USA 1987, 84, 5087-5091.

18. Toniolo, C.; Peggion, C.; Crisma, M.; Formaggio, F.; Shui, X.; Eggleston, D. S. Nat Struct Biol 1994, 1, 908-914.

19. Crisma, M.; Monaco, V.; Formaggio, F.; Toniolo, C.; George, C.; Flippen-Anderson, J. L. Lett Pept Sci 1997, 4, 213-218.

20. Topical Issue: Peptaibiotics; Toniolo, C.; Brückner, H., Eds.; Chem Biodivers, 2007, 4, No. 6.

21. Topical Issue: Peptaibiotics II; Brückner, H.; Toniolo, C., Eds.; Chem Biodivers, 2013, 10, No. 5.

22. Toniolo, C.; Brückner, H. Peptaibiotics: Fungal Peptides Containing α-Dialkyl α-Amino Acids, Wiley-VCH, Weinheim, 2009.

23. Toniolo, C.; Crisma, M.; Formaggio, F.; Peggion, C. Biopolymers (Pept Sci) 2001, 60, 396-419.

24. Karle, I.L.; Balaram, P. Biochemistry 1990, 29, 6747-6756.

25. Toniolo, C.; Crisma, M.; Formaggio, F. Biopolymers 1998, 47, 153-158.

26. Hanson, P.; Millhauser, G.; Formaggio, F.; Crisma, M.; Toniolo, C. J Am Chem Soc 1996, 118, 7618-7625.

27. Hanson, P.; Anderson, D.J.; Martinez, G.; Millhauser, G.; Formaggio, F.; Crisma, M.; Toniolo, C.; Vita, C. Mol Phys 1998, 95, 957-966.

28. Anderson, D. J.; Hanson, P.; Mc Nulty, J.; Millhauser, G. L, Monaco, V.; Formaggio, F.; Crisma, M.; Toniolo, C. J Am Chem Soc 1999, 121, 6919-6927.

29. Bobone, S.; Roversi, D.; Giordano, L.; De Zotti, M.; Formaggio, F.; Toniolo, C.; Park, Y.; Stella, L. Biochemistry 2012, 51, 10124-10126.

30. Bobone, S.; Gerelli, Y.; De Zotti, M.; Bocchinfuso, G.; Farrotti, A.; Orioni, B.; Sebastiani, F.; Latter, E.; Penfold, J.; Senesi, R.; Formaggio, F.; Palleschi, A.; Toniolo, C.; Fragneto, G.; Stella, L. Biochim Biophys Acta (Biomembr.) 2013, 1828, 1013–1024.

31. Milov, A.D.; Maryasov, A.G.; Tsvetkov, Yu.D. Appl Magn Reson 1998, 15, 107-143.

32. Maryasov, A.G.; Tsvetkov, Yu.D. Appl Magn Reson 2000, 18, 583-605.

33. Ponomarev, A.V.; Milov, A.D.; Tsvetkov, Yu.D. J Struct Chem (Russian) 1984, 25, 51-54.

34. Milov, A.D.; Ponomarev, A.V.; Tsvetkov, Yu.D. Chem Phys Lett 1984, 110, 67-72.

35. Parmon, V.N.; Kokorin, A.I.; Zhidomirov, G.M. Stable Biradicals (Russian), Nauka, Moscow, 1980.

36. Tikhonov, A.N.; Arsenin, V.Y. Solutions of Ill-Posed Problems, Wiley, New York, 1977.

37. Bowman, M.K.; Maryasov, A.G.; Kim, N.; DeRose, V.J. Appl Magn Reson 2004, 26, 23-29.

38. Jeschke, G.; Koch, A.; Jonas, U.; Godt, A. J Magn Reson 2002, 155, 72-82.

39. Jeschke, G.; Panek, G.; Godt, A.; Bender, A.; Paulsen, H. Appl Magn Reson 2004, 26, 223-244.

40. Chiang, Y.-W.; Borbat, P.P.; Freed, J.H. J Magn Reson 2005, 172, 279-295.

41. Jeschke, G.; Sajid, M.; Schulte, M.; Godt, A. PhysChemChemPhys 2009, 11, 6580-6592.

42. Jeschke, G.; Chechik, V.; Ionita, P.; Godt, A.; Zimmermann, H.; Banham, J.; Timmel, C.R.; Hilger, D.; Jung, H. Appl Magn Reson 2006, 30, 473-498.

43. Milov, A.D.; Samoilova, R.I.; Tsvetkov, Yu.D.; Gusev, V.A.; Formaggio, F.; Crisma, M.; Toniolo, C.; Raap, J. Appl Magn Reson 2002, 23, 81-95.

44. Tsvetkov, Yu.D. In Biological Magnetic Resonance, vol. 21 (EPR: Instrumental Methods); Bender, C.J.; Berliner, L.J.; Kluwer/Plenum Press: New York, 2004; pp 385-434.

45. Milov, A.D.; Tsvetkov, Yu.D.; Maryasov, A.G.; Gobbo, M.; Prinzivalli, C.; De Zotti, M.; Formaggio, F.; Toniolo, C. Appl Magn Reson 2013, 44, 495-508.

46. Salikhov, K.M.; Khairuzhdinov, I.T. Appl Magn Reson 2015, 46, 67-83.

47. Salikhov, K.M.; Khairuzhdinov, I.T.; Zaripov, R.B. Appl Magn Reson 2014, 45, 573-619.

48. Milov, A.D.; Tsvetkov, Yu.D.; Gorbunova, E.Yu.; Mustaeva, L.G.; Ovchinnikova, T.V.; Raap, J. Biopolymers 2002, 64, 328-336.

49. Milov, A.D.; Tsvetkov, Yu.D.; Gorbunova, E.Y.; Mustaeva, L.G.; Ovchinnikova, T.V.; Handgraaf, J.-W.; Raap, J. Chem Biodivers 2007, 4, 1243-1255.

50. Toniolo, C.; Benedetti, E. Trends Biochem Sci 1991, 16, 350-353.

51. Yasui, S.C.; Keiderling, T.A.; Bonora, G.M.; Toniolo, C. Biopolymers 1986, 25, 79-89.

52. Crisma, M.; Formaggio, F.; Moretto, A.; Toniolo, C. Biopolymers (Pept Sci) 2006, 84, 3-12.

53. Toniolo, C. CRC Crit Rev Biochem 1980, 9, 1-44.

54. Crisma, M.; De Zotti, M.; Moretto, A.; Peggion, C.; Drouillat, B.; Wright, K.; Couty, F.; Toniolo, C.; Formaggio, F. New J Chem 2015, 39, 3208-3216.

55. Armen, R.; Alonso, D.O.V.; Daggett, V. Protein Sci 2003, 12, 1145-1157.

56. Millhauser, G. L. Biochemistry 1995, 34, 3873-3877.

57. Pengo, P.; Pasquato, L.; Moro, S.; Brigo, A.; Fogolari, F.; Broxterman, Q. B.; Kaptein, B.; Scrimin, P.; Angew Chem Int Edit 2003, 42, 3388-3392.

58. Milov, A.D.; Maryasov, A.G.; Tsvetkov, Yu.D.; Raap, J. Chem Phys Lett 1999, 303, 135-143.

59. Milov, A.D.; Maryasov, A.G.; Samoilova R.I.; Tsvetkov, Yu.D., Raap, J.; Monaco, V.; Formaggio, F.; Crisma, M.; Toniolo, C. Dokl Acad Nauk (Russian) 2000, 370, 265-268.

60. Milov, A.D.; Tsvetkov, Yu.D.; Formaggio F.; Crisma, M.; Toniolo, C.; Raap, J. J Am Chem Soc 2001, 123, 3784-3789.

61. Milov, A.D.; Tsvetkov, Yu.D.; Maryasov, A.G.; Gobbo, M.; Prinzivalli, C.; De Zotti, M.; Formaggio, F.; Toniolo, C. Appl Magn Reson 2013, 44, 495-508.

62. Milov, A.D.; Tsvetkov, Yu.D.; De Zotti, M.; Prinzivalli, C.; Biondi, B.; Formaggio, F.; Toniolo, C.; Gobbo, M. J Struct Chem 2013, 54, S73-S85.

63. Milov, A.D.; Tsvetkov, Yu.D.; Bortolus, M.; Maniero, A.L.; Gobbo, M.; Toniolo, C.; Formaggio, F. J Pept Sci 2013, 102, 40-48.

64. Peggion, C; Jost, M.; Baldini, C.; Formaggio, F.; Toniolo, C. Chem Biodivers 2007, 4, 1183-1199.

65. Milov, A.D.; Samoilova, R.I.; Tsvetkov, Yu.D.; De Zotti, M.; Toniolo, C.; Raap, J. J Phys Chem B 2008, 112, 13469-13472.

66. Milov, A.D.; Tsvetkov, Yu.D.; Formaggio, F.; Oancea, S.; Toniolo, C.; Raap, J. J Phys Chem 2003, 107, 13719-13727.

67. Milov, A.D.; Tsvetkov, Yu.D.; Formaggio, F.; Oancea, S.; Toniolo, C.; Raap, J. PhysChemChemPhys 2004, 6, 3596-3603.

68. Rabenstein, M.D.; Shin, Y.K. Proc Natl Acad Sci USA 1995, 92, 8239-8243.

69. Bortolus, M.; Tombolato, F.; Tessari, I.; Bisaglia, M.; Mammi, S.; Bubacco, L.; Ferrarini, A.; Maniero, A.L. J Am Chem Soc 2008, 130, 6690-6691.

70. Karle, I.L. In Membrane Protein Structure: Experimental Approaches; White, S.H., Ed.; Oxford University Press: Oxford, 1994, pp 355-380.

71. Balashova, T.A.; Shenkarev, Z.O.; Tagaev, A.A.; Ovchinnikova, T.V.; Raap, J.; Arseniev, A.S. FEBS Lett 2000, 466, 333-336.

72. Peggion, C.; Coin, I.; Toniolo, C. Biopolymers (Pept Sci) 2004, 76, 485-493.

73. Crisma, M.; Peggion, C.; Baldini, C.; MacLean, E.J.; Vedovato, N.; Rispoli, G.; Toniolo, C. Angew Chem Int Edit 2007, 46, 2047-2050.

74. Milov, A.D.; Tsvetkov, Yu.D.; Formaggio F.; Crisma, M.; Toniolo, C.; Raap, J. J Am Chem Soc 2000, 122, 3843-3848.

75. Milov, A.D.; Samoilova, M.I.; Tsvetkov, Yu.D.; Peggion, C.; Formaggio, F.; Toniolo, C.; Raap, J. Dokl Akad Nauk (Russian) 2006, 406, 21-25.

76. Milov, A.D.; Salmoilova, R.I.; Tsvetkov, Yu.D.; Jost, M.; Peggion, C.; Formaggio, F.; Crisma, M.; Toniolo, C.; Handgraaf, J.-W.; Raap, J. Chem Biodivers 2007, 4, 1275-1298.

77. Milov, A.D.; Tsvetkov, Yu.D.; Raap, J. Appl Magn Reson 2000, 19, 215-226.

78. Milov, A.D.; Tsvetkov, Yu.D.; Formaggio, F.; Crisma, M.; Toniolo, C.; Raap, J. J Pept Sci 2003, 9, 690-700.

79. Milov, A.D.; Tsvetkov, Yu.D.; Formaggio, F.; Crisma, M.; Toniolo, C.; Millhauser, G.L.; Raap, J. J Phys Chem B 2001, 105, 11206-11213.

80. Marsh, D. In Biological Magnetic Resonance; Berliner, L.J.; Reuben, J., Eds.; Plenum Press: New York, 1989; pp 255-303.

81. Stella, L.; Mazzuca, C.; Venanzi, M.; Palleschi, A.; Didoné, M.; Formaggio, F.; Toniolo, C.; Pispisa, B. Biophys J 2004, 86, 936-945.

82. Kropacheva, T. N.; Raap, J. Biochim Biophys Acta 2002, 1567, 193-203.

83. Milov, A. D.; Samoilova, R. I.; Tsvetkov, Yu. D.; Formaggio, F.; Toniolo, C.; Raap, J. Appl Magn Reson 2005, 29, 703-716.

84. Salnikov, E.S.; Erilov, D.A.; Milov, A.D.; Tsvetkov, Yu.D.; Peggion, C.; Formaggio, F.; Toniolo, C.; Raap, J.; Dzuba, S.A. Biophys J 2006, 91, 1532-1540.

85. Milov, A.D.; Erilov, D.A.; Salnikov, E.S.; Tsvetkov, Yu.D.; Formaggio, F.; Toniolo, C.; Raap, J. PhysChemChemPhys 2005, 7, 1794-1799.

86. Doig, A. J.; Chakrabartty, A.; Klinger, T. M.; Baldwin, R. L. Biochemistry 1994, 33, 3396-3403.

87. Syryamina, V.N.; De Zotti, M.; Peggion, C.; Formaggio, F.; Toniolo, C.; Raap, J.; Dzuba, S.A. J Phys Chem B 2012, 116, 5653−5660.

88. Becucci, L.; Maran, F.; Guidelli, R. Biochim Biophys Acta 2012, 1818, 1656-1662.

89. Smeazzetto, S.; De Zotti, M.; Moncelli, M.R. Electrochem Commun 2011, 13, 834-836.

90. Milov, A.D.; Samoilova, R.I.; Tsvetkov, Yu.D.; Formaggio, F.; Toniolo, C.; Raap, J. J Am Chem Soc 2007, 129, 9260-9261.

91. Bartucci, R.; Guzzi, R.; De Zotti, M.; Toniolo, C.; Sportelli, L.; Marsh, D. Biophys J 2008, 94, 2698-2705.

92. Salnikov, E.S.; De Zotti, M.; Formaggio, F.; Li, X.; Toniolo, C.; O' Neil, J.D.J.; Raap, J.; Dzuba, S.A.; Bechinger, B. J Phys Chem B 2009, 113, 3034-3042.

93. Milov, A.D.; Samoilova, R.I.; Tsvetkov, Yu.D.; De Zotti, M.; Formaggio, F.; Toniolo, C.; Handgraaf, J.-W.; Raap, J. Biophys J 2009, 96, 3197-3209.

94. North, C.L.; Barranger-Mathys, M.; Cafiso, D.S. Biophys J 1995, 69, 2392-2397.

95. Salnikov, E.S.; Friedrich, H.; Li, X.; Bertani, P.; Reissmann, S.; Hertweck, C.; O'Neil, J.D.J.; Raap, J.; Bechinger, B. Biophys J 2009, 96, 86-100.

96. Marsh, D.; Jost, M.; Peggion, C.; Toniolo, C. Biophys J 2007, 92, 4002-4011.

97. Parsegian, V.A.; Fuller, N.; Rand, R.P. Proc Natl Acad Sci USA 1979, 76, 2750-2754.

98. Murzyn, K.; Rog, T.; Blicharski, W.; Dutka, M.; Pyka, J.; Szytula, S.; Froncisz, W. Proteins: Struct Funct Bioinform 2006, 62, 1088-1100.

99. Spaar, A.; Münster, C.; Salditt, T. Biophys J 2004, 87, 396-407.

100. Whiteside, T.L.; De Siervo, A.J.; Salton, M.R.J. J Bacteriol 1971, 105, 957-967.

101. Thorne, K.J.; Kodicek, E. Biochim Biophys Acta 1962, 59, 306-312.

102. Salton, M.R.J. The Bacterial Cell Wall, Elsevier, Amsterdam, 1964.